© 2019. Published by The Company of Biologists Ltd | Journal of Cell Science (2019) 132, jcs234195. doi:10.1242/jcs.234195

RESEARCH ARTICLE

The RBG-1–RBG-2 complex modulates autophagy activity by regulating lysosomal biogenesis and function in *C. elegans*

Zhaoyu Wang[1], Hongyu Zhao[1], Chongzhen Yuan[1], Dongfeng Zhao[1], Yanan Sun[1], Xiaochen Wang[1,2] and Hong Zhang[1,2,*]

ABSTRACT

Vici syndrome is a severe and progressive multisystem disease caused by mutations in the *EPG5* gene. In patient tissues and animal models, loss of *EPG5* function is associated with defective autophagy caused by accumulation of non-degradative autolysosomes, but very little is known about the mechanism underlying this cellular phenotype. Here, we demonstrate that loss of function of the RBG-1–RBG-2 complex ameliorates the autophagy defect in *C. elegans epg-5* mutants. The suppression effect is independent of the complex's activity as a RAB-3 GAP and a RAB-18 GEF. Loss of *rbg-1* activity promotes lysosomal biogenesis and function, and also suppresses the accumulation of non-functional autolysosomes in *epg-5* mutants. The mobility of late endosome- and lysosome-associated RAB-7 is reduced in *epg-5* mutants, and this defect is rescued by simultaneous loss of function of *rbg-1*. Expression of the GDP-bound form of RAB-7 also promotes lysosomal biogenesis and suppresses the autophagy defect in *epg-5* mutants. Our study reveals that the RBG-1–RBG-2 complex acts by modulating the dynamics of membrane-associated RAB-7 to regulate lysosomal biogenesis, and provides insights into the pathogenesis of Vici syndrome.

KEY WORDS: RBG-1, RAB3GAP1, *epg-5*, RAB-7, Lysosome, Autophagy, *C. elegans*

INTRODUCTION

Multiple aspects of intracellular vesicle trafficking such as vesicle budding, transport, tethering and fusion are controlled by RAB small GTPases (Stenmark, 2009; Wandinger-Ness and Zerial, 2014). RAB proteins cycle between GTP-bound active and GDP-bound inactive forms, accompanied by membrane association and dissociation (Stenmark, 2009; Mizuno-Yamasaki et al., 2012; Blümer et al., 2013; Wandinger-Ness and Zerial, 2014). Guanine nucleotide exchange factors (GEFs) mediate the exchange of GDP for GTP, which in turn recruits downstream effectors (Stenmark, 2009; Mizuno-Yamasaki et al., 2012; Blümer et al., 2013; Wandinger-Ness and Zerial, 2014), whereas GTPase-activating proteins (GAPs) stimulate GTP hydrolysis to terminate the RAB effect (Stenmark, 2009; Mizuno-Yamasaki et al., 2012; Blümer et al., 2013; Wandinger-Ness and Zerial, 2014). GDP-dissociation inhibitors (GDIs) facilitate the extraction of membrane-associated GDP-bound RAB proteins into the cytosol. Targeting of the cytosolic RAB–GDI complex onto cognate membranes requires membrane-bound GDI displacement factors (GDFs) and also GEFs (Stenmark, 2009; Mizuno-Yamasaki et al., 2012; Blümer et al., 2013; Wandinger-Ness and Zerial, 2014). The cycling of RAB proteins between their GTP- and GDP-bound forms is critical for membrane dynamics. The concerted actions of GEF and GAP proteins ensure tight spatiotemporal control of the activity of RAB proteins in membrane trafficking (Stenmark, 2009; Mizuno-Yamasaki et al., 2012). RAB7 is located on late endosomes and lysosomes and participates in diverse dynamic membrane-based processes through the recruitment of different effector proteins. These processes including maturation of early endosomes to late endosomes, membrane fusion of late endosomes (homotypic fusion and also heterotypic fusion of late endosomes with lysosomes), lysosomal biogenesis, and positioning of late endosomes and lysosomes (Bucci et al., 2000; Hyttinen et al., 2013; Guerra and Bucci, 2016; Langemeyer et al., 2018). Little is known about the factors that regulate the dynamics of membrane-associated RAB7 to control lysosomal biogenesis.

Macroautophagy (hereafter referred to as autophagy) involves the formation of a double-membrane autophagosome, and its delivery to lysosomes (metazoans) or the vacuole (yeast) for degradation of sequestrated materials (Nakatogawa et al., 2009; Feng et al., 2014). In multicellular organisms, nascent autophagosomes fuse with endolysosomal vesicles to form amphisomes, a process known as autophagosome maturation, before eventually forming degradative autolysosomes (Zhao and Zhang, 2019). Upon degradation of sequestrated materials, lysosomes regenerate from autolysosomes to maintain lysosome homeostasis (Yu et al., 2010). Autophagosome maturation requires the concerted actions of RAB small GTPases, tethering factors and the SNARE complex (Zhao and Zhang, 2019). Fusion of autophagosomes with late endosomes and lysosomes is driven by the STX17–SNAP29–VAMP8 (VAMP7 in fly and worm) and YKT6–SNAP29–STX7 SNARE complexes (Itakura et al., 2012; Jiang et al., 2014; McEwan et al., 2015; Bas et al., 2018; Gao et al., 2018b; Matsui et al., 2018). The dynamics of GTP- and GDP-bound RAB7 is essential for formation of functional autolysosomes (Zhao and Zhang, 2019). Activated RAB7 recruits tethering factors such as PLEKHM1 and the HOPS complex to late endosomes and lysosomes to promote the stability and assembly of the trans-SNARE complex, mediating autophagosome–lysosome fusion (Jiang et al., 2014; McEwan et al., 2015). RAB7 is also targeted to autophagosomes by its GEF, the MON1–CCZ1 complex, which is recruited to autophagosomes via direct interaction with ATG8 to promote fusion of autophagosomes with lysosomes and vacuoles (Hegedus et al., 2016; Vaites et al., 2017; Gao et al., 2018a). Inactivation of RAB7 by TBC-domain-containing RAB GAP protein Armus (TBC1D2), which is targeted to autophagosomes via interaction

[1]National Laboratory of Biomacromolecules, CAS Center for Excellence in Biomacromolecules, Institute of Biophysics, Chinese Academy of Sciences, Beijing 100101, China. [2]College of Life Sciences, University of Chinese Academy of Sciences, Beijing 100049, China.

*Author for correspondence (hongzhang@ibp.ac.cn)

C.Y., 0000-0003-1520-4148; D.Z., 0000-0002-0044-6454; H.Z., 0000-0003-0849-7026

Received 12 May 2019; Accepted 19 August 2019

Journal of Cell Science (2019) 132, jcs234195. doi:10.1242/jcs.234195

with the LC3 (MAP1LC3) protein family, also facilitates autophagosome maturation (Carroll et al., 2013).

The metazoan-specific autophagy protein EPG5 functions as a tethering factor to confer the fusion specificity of autophagosomes with late endosomes and lysosomes (Tian et al., 2010; Wang et al., 2016). EPG5 is a RAB7 effector and localizes on late endosomes and lysosomes. It directly interacts with autophagosomal-localized LC3 and facilitates assembly of the STX17–SNA29–VAMP8 SNARE complex (Wang et al., 2016). Loss of *EPG5* function causes non-specific fusion of autophagosomes with other endocytic vesicles such as recycling endosomes, resulting in the formation of non-degradative autolysosomes (Wang et al., 2016). In addition to autophagy, EPG5 is essential for endocytic recycling and degradation (Zhao et al., 2013a). *EPG5* knockdown slows endocytic degradation and delays endocytic recycling (Zhao et al., 2013a). Recessive mutations in human *EPG5* are causatively linked to the multisystem disorder Vici syndrome, key features of which include agenesis of the corpus callosum, myopathy and combined immunodeficiency (Dionisi et al., 1998; Cullup et al., 2013). *Epg5* knockout (KO) mice display some phenotypic similarities with individuals with Vici syndrome, including corpus callosum changes and myopathy (Zhao et al., 2013a,b). *Epg5* KO mice, however, exhibit elevated basal lung inflammation (Lu et al., 2016). Accumulation of non-degradative autolysosomes has been observed in Vici syndrome patient tissues, in *epg-5*-depleted *C. elegans* and in *Epg5*-deficient mice (Cullup et al., 2013; Zhao et al., 2013a; Wang et al., 2016), but the mechanism underlying this accumulation remains unknown.

Here, we demonstrate that loss of function of *rbg-1* and *rbg-2*, encoding RBG-1 and RBG-2 (RAB3GAP1 and RAB3GAP2 in mammals), respectively, ameliorates the autophagy defect in *C. elegans epg-5* mutants. RAB3GAP1 and RAB3GAP2 form a complex that acts as a GAP for RAB3 and a GEF for RAB18 (Fukui et al., 1997; Nagano et al., 1998; Gerondopoulos et al., 2014). Loss of *rbg-1* activity facilitates lysosomal biogenesis and function in a manner independent of its catalytic activity on RAB-3 and RAB-18. The reduced dynamics of membrane-associated RAB-7 and accumulation of non-degradative autolysosomes in *epg-5* mutants are suppressed by simultaneous inactivation of *rbg-1*. Expression of the GDP-bound form of RAB-7 has the same effect as loss of function of *rbg-1* activity on lysosomal biogenesis and *epg-5* suppression. Our results indicate that RBG-1 regulates RAB-7 cycling to modulate lysosomal biogenesis and function.

RESULTS

Genetic screens identify mutations suppressing the autophagy defect in *epg-5* mutants

To investigate the mechanism underlying the accumulation of non-degradative autolysosomes in *epg-5* mutants, we performed genetic screens to identify mutations that suppress the accumulation of aggregates of the *C. elegans* p62 (also known as SQSTM1) homolog SQST-1 in *epg-5(tm3425)* null mutants. The *bpIs267* line, in which SQST-1::GFP is specifically expressed in the hypodermis, was used to facilitate the screen. In wild-type animals, SQST-1::GFP is weakly expressed and diffusely localized in the cytoplasm (Fig. 1A,B), while in *epg-5* mutants a large number of SQST-1 aggregates accumulate throughout development (Fig. 1C). From EMS screens, a mutation, *bp1150*, was isolated that dramatically reduced the number of SQST-1::GFP aggregates in *epg-5* mutants (Fig. 1D,E). Accumulation of SQST-1::GFP aggregates was also suppressed by *bp1150* in *epg-5* mutants with transgenic expression of SQST-1 in other tissues, including the whole body using the endogenous *sqst-1* promoter (P*sqst-1*::SQST-1::GFP), the intestine (P*ges-1*::SQST-1::GFP), muscle (P*hlh-1*::SQST-1::GFP) and neurons (P*unc-119*::SQST-1::GFP) (Fig. S1A–Y). Compared to *epg-5* single mutants, accumulation of endogenous autophagy substrates, including SQST-1 and components of PGL granules, was also dramatically reduced in *epg-5; bp1150* mutants (Fig. 1F–J; Fig. S1Z–I1). SQST-1::GFP aggregates in *epg-5; bp1150* mutants were restored by simultaneous loss of autophagy activity, such as that caused by loss of *lgg-1*, the *C. elegans* homolog of Atg8 (GABARAP in vertebrates) (Fig. 1K–O). This suggests that the *bp1150* mutation promotes autophagic degradation of SQST-1 in an EPG-5-independent manner during development.

A large number of non-degradative autophagic structures labeled by LGG-1 accumulate in *epg-5* mutants (Tian et al., 2010). Accumulation of LGG-1 puncta in *epg-5* mutant embryos and also in the hypodermis and intestine of *epg-5* mutant larvae was reduced in animals also harboring the *bp1150* mutation (Fig. 1P–T; Fig. S1J1–S1). Taken together, these results indicate that *bp1150* suppresses the autophagy defect in *epg-5* mutants.

bp1150 encodes the *rbg-1* homolog

We cloned the *bp1150* mutation by transformation rescue experiments. A transgene expressing *rbg-1* restored the accumulation of SQST-1::GFP aggregates in *epg-5; bp1150* hypodermal cells (Fig. 2A–D). The *bp1150* mutation was determined to contain a tryptophan-to-stop codon mutation at residue 718 in RBG-1 (Fig. S2A), and the mutation is hereafter termed *rbg-1(bp1150)*. *rbg-1(RNAi)* also reduced SQST-1::GFP aggregates in *epg-5* mutants (Fig. S2B), indicating that the suppression effect was caused by loss of *rbg-1* activity. RBG-1 forms a complex with RBG-2. *rbg-2(RNAi)* suppressed the accumulation of SQST-1::GFP aggregates in *epg-5* mutants (Fig. 2E–H; Fig. S2C,D), suggesting that RBG-1 functions with RBG-2 to regulate the degradation of autophagy substrates in *epg-5* mutants.

The RAB3GAP1–RAB3GAP2 complex acts as a GAP for RAB3 and a GEF for RAB18 (Fukui et al., 1997; Nagano et al., 1998; Gerondopoulos et al., 2014). Transgenes expressing RBG-1(R667A), which impairs the RAB3 GAP activity, or RBG-1(T16P) and RBG-1(E22V), which disrupt the RAB18 GEF activity, retained rescuing activity (Fig. 2I–L). Loss of function of *rab-3* and *rab-18* failed to restore the accumulation of SQST-1::GFP aggregates in *epg-5; rbg-1* mutants (Fig. S2E), and did not reduce the number of SQST-1::GFP aggregates in *epg-5* mutants (Fig. S2F). These results indicate that loss of *rbg-1* activity suppresses the autophagy defect in *epg-5* mutants in a RAB-3- and RAB-18-independent manner.

Loss of *rbg-1* activity suppresses the autophagy defect in some mutants with impaired lysosomal function

We next examined whether loss of function of *rbg-1* suppresses the autophagy defect in other autophagy mutants with phenotypes that can be suppressed by enhanced autophagy activity, such as through mTOR inactivation. Loss of function of *epg-7*, which encodes the scaffold protein facilitating degradation of SQST-1, caused accumulation of SQST-1::GFP aggregates (Lin et al., 2013). *rpl-43(bp399)* mutants, which display impaired function of the ribosomal protein RPL-43, accumulate SQST-1::GFP aggregates in the intestine (Guo et al., 2014); however, SQST-1::GFP aggregates in both *epg-7* and *rpl-43* mutant larvae are suppressed by elevated autophagy activity (Lin et al., 2013; Guo et al., 2014). The *rbg-1(bp1150)* mutation did not reduce the number of SQST-1::GFP aggregates in *epg-7* or *rpl-43* mutants (Fig. S3A,B). Simultaneous depletion of *rbg-1* did not suppress, but instead slightly increased, the

Journal of Cell Science (2019) 132, jcs234195. doi:10.1242/jcs.234195

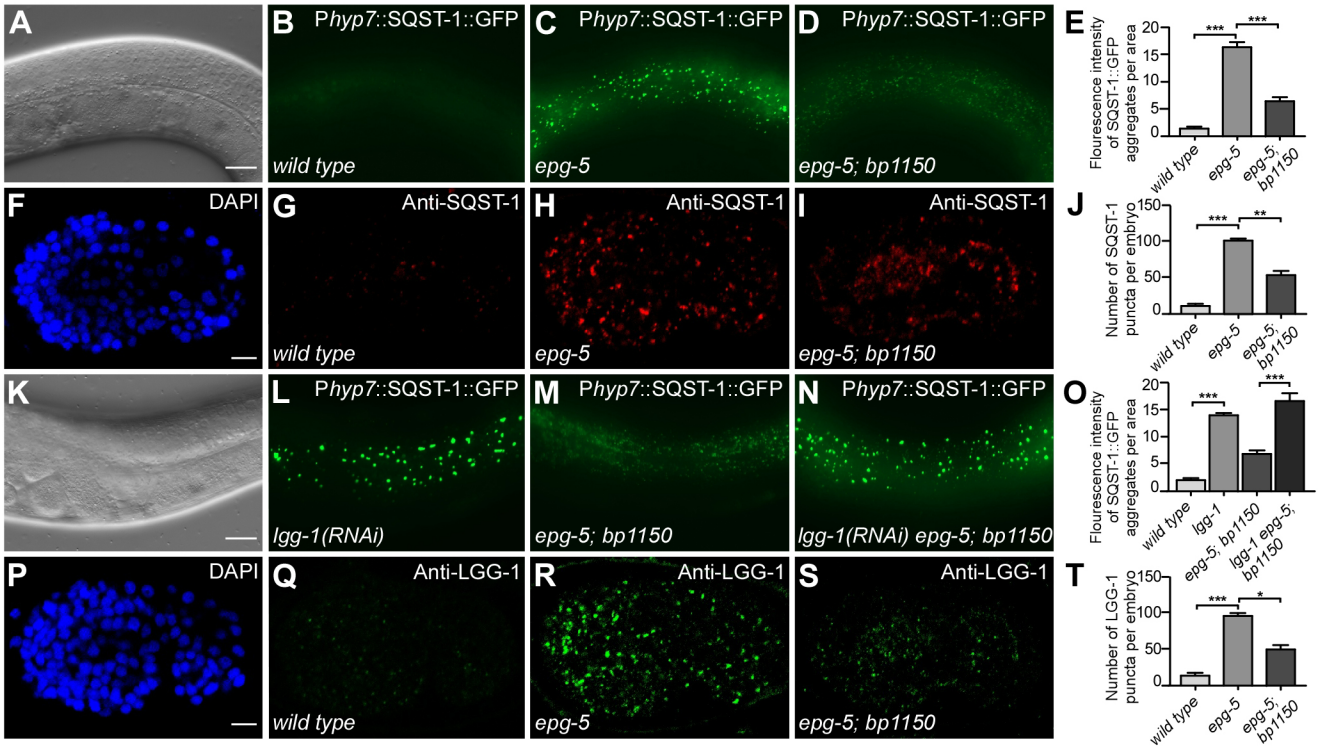

Fig. 1. *bp1150* mutation suppresses the autophagy defect in *epg-5* mutants. (A–E) In wild-type hypodermis, SQST-1::GFP is weakly expressed and diffusely localized (B). (A) Differential interference contrast (DIC) image of the animal in B. A large number of SQST-1::GFP aggregates accumulate in *epg-5* hypodermis (C), and this is largely suppressed in *epg-5; bp1150* double mutants (D). Young adult stage animals are shown. (E) Quantification of the fluorescence intensity of SQST-1::GFP in wild type, *epg-5* mutants and *epg-5; bp1150* mutants is shown as mean±s.e.m. (n=10). 'Area' used for quantification refers to the captured image. ***P<0.001 (two-tailed t-test). Scale bar: 20 µm (A–D). (F–J) Endogenous SQST-1, detected by anti-SQST-1 antibody (diluted 1:1000), is absent in wild-type embryos at the comma stage (G). (F) DAPI image of the embryo in G. SQST-1 accumulates into numerous aggregates in *epg-5* mutant embryos (H), and this is largely suppressed in *epg-5; bp1150* embryos (I). (J) Quantification of the number of SQST-1 puncta in wild type, *epg-5* mutants and *epg-5; bp1150* mutants is shown as mean±s.e.m. (n=3). **P<0.01, ***P<0.001 (two-tailed t-test). Scale bar: 5 µm (F–I). (K–O) SQST-1::GFP aggregates accumulate in *lgg-1(RNAi)* animals (L). (K) DIC image of the animal in L. *lgg-1(RNAi)* (N) restores the SQST-1::GFP accumulation in *epg-5; bp1150* animals (M). (O) Quantification of the fluorescence intensity of SQST-1::GFP in wild-type, *lgg-1(RNAi)*, *epg-5; bp1150* and *epg-5; bp1150; lgg-1(RNAi)* animals is shown as mean±s.e.m. (n=5). ***P<0.001 (two-tailed t-test). Scale bar: 20 µm (K–N). (P–T) LGG-1, detected by anti-LGG-1 antibody (diluted 1:1000), does not form puncta in wild-type embryos at the comma stage (Q). (P) DAPI image of the embryo in Q. LGG-1 puncta dramatically accumulate in *epg-5* mutant embryos (R). The number of LGG-1 puncta is dramatically decreased in *epg-5; bp1150* embryos (S). (T) Quantification of the number of LGG-1 puncta in wild type, *epg-5* mutants and *epg-5; bp1150* mutants is shown as mean±s.e.m. (n=3). *P<0.05, ***P<0.001 (two-tailed t-test). Scale bar: 5 µm (P–S).

SQST-1::GFP aggregates in *bec-1(bp613)* mutants, which exhibit partially impaired function of the *C. elegans* homolog of BECN1. (Fig. 2M–P). This is consistent with a previous study showing that loss of *rbg-1* activity causes a mild autophagy defect (Spang et al., 2014).

We also determined whether loss of *rbg-1* activity ameliorates the accumulation of SQST-1 aggregates caused by impaired lysosomal function. The number of SQST-1::GFP aggregates in mutants of *cpl-1*, encoding cathepsin L, was reduced in larvae also harboring the *rbg-1(bp1150)* mutation (Fig. 2Q–T). *rbg-1(RNAi)* failed to suppress the autophagy defect in mutants of *scav-3* (Fig. S3C), which encodes a lysosomal membrane protein involved in maintaining lysosome integrity (Li et al., 2016). Thus, loss of *rbg-1* activity appears to suppress the autophagy defect resulting from impaired lysosomal degradation.

Loss of function of *rbg-1* promotes lysosomal activity

The specific alleviation of the autophagy defect in *epg-5* and *cpl-1* mutants by loss of *rbg-1* prompted us to examine lysosome biogenesis in *rbg-1* mutants. mCherry-tagged lysosomal-localized DNase II NUC-1 and the late endosome marker GFP::RAB-7 label spherical structures in the wild-type hypodermis (Fig. 3A; Fig. S3D). In *rbg-1* animals, NUC-1::mCherry and GFP::RAB-7 labeled spherical and tubular structures that were smaller and more abundant than those in wild-type animals (Fig. 3B,M,N; Fig. S3E). Ultrastructural analysis by transmission electron microscopy (TEM) also revealed that lysosomes in the hypodermis in *rbg-1* mutants were smaller than those in wild-type animals (Fig. 3E,F).

We performed time-lapse analysis of the delivery of the sfGFP::mCherry tandem-tagged NUC-1 to monitor the transport of lysosomal enzymes. The NUC-1::sfGFP::mCherry reporter is driven by the heat shock promoter. The animals carrying this reporter are heat-shocked at 33°C for 30 min and then shifted to 20°C. The newly synthesized NUC-1 produces both red and green fluorescent signals. The GFP signal is quenched inside acidic lysosomes, and thus red-only signals represent acidified lysosomal structures. In wild-type animals, NUC-1::sfGFP::mCherry was detected 2 h after heat shock (Fig. 4A). The number of yellow puncta gradually decreased after 12 h and only red puncta persisted after 24 h (Fig. 4B–E,E1). In *rbg-1* mutants, the number of yellow puncta was similar to that in wild-type animals at 2 h after heat shock (Fig. 4F,E1), but the number of red-only puncta was significantly higher at 8 and 12 h after heat shock (Fig. 4G–J,E1). These results indicate that loss of *rbg-1* activity accelerates the delivery of NUC-1::

Journal of Cell Science (2019) 132, jcs234195. doi:10.1242/jcs.234195

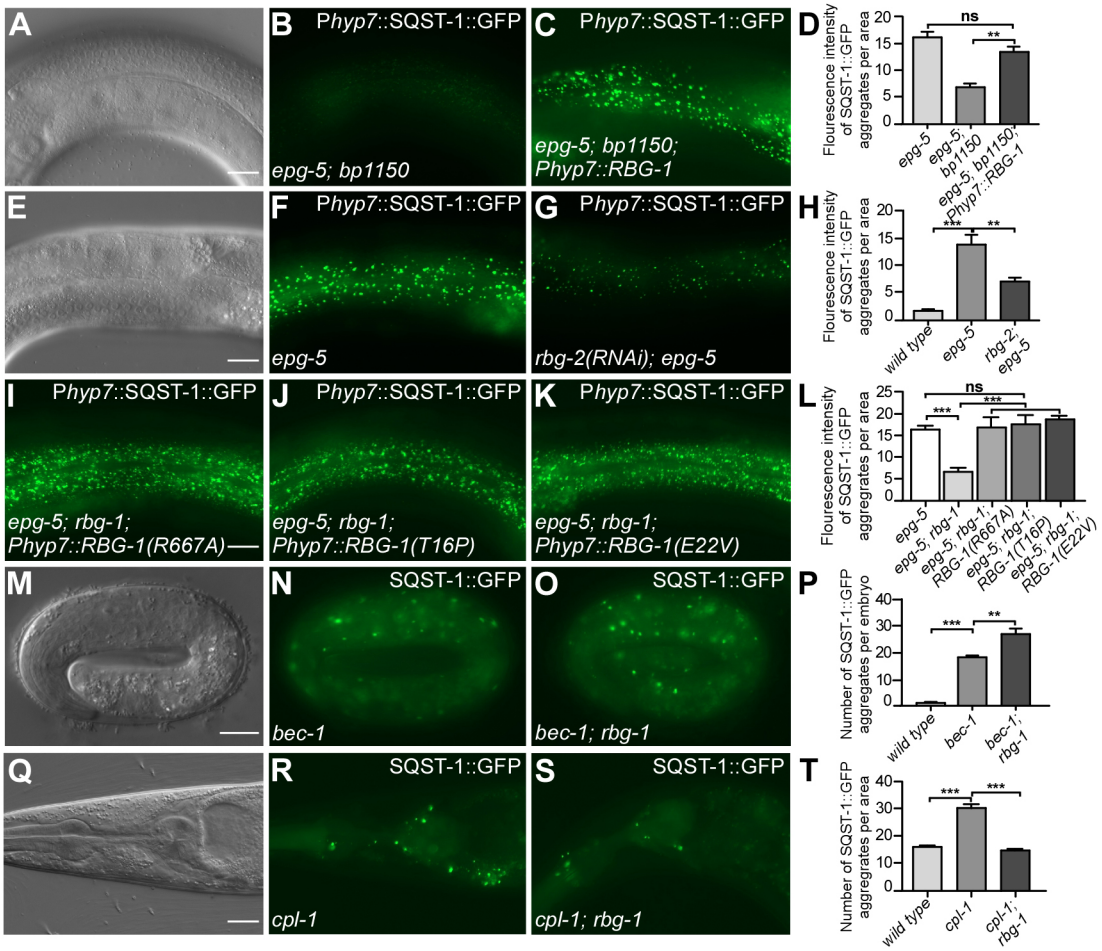

Fig. 2. Loss of *rbg-1* and *rbg-2* activity suppresses the autophagy defect in *epg-5* mutants. (A–D) Expression of *rbg-1* in the hypodermis restores the SQST-1::GFP accumulation in *epg-5; bp1150* mutants (C). (A) DIC image of the animal in B. (D) Quantification of the fluorescence intensity of SQST-1::GFP in *epg-5*, *epg-5; bp1150* and *epg-5; bp1150; Phyp7::RBG-1* is shown as mean±s.e.m. (*n*=5). ***P*<0.01 (two-tailed *t*-test); ns, no significant difference. Scale bar: 20 µm (A–C). (E–H) *rbg-2(RNAi)* suppresses the accumulation of SQST-1::GFP aggregates in *epg-5* mutants (G). (E) DIC image of the animal in F. (H) Quantification of the fluorescence intensity of SQST-1::GFP in wild-type, *epg-5* and *rbg-2(RNAi); epg-5* animals is shown as mean±s.e.m. (*n*=8). ***P*<0.01, ****P*<0.001 (two-tailed *t*-test). Scale bar: 20 µm (E–G). (I–L) Expression of mutant RBG-1(R667A) (I), RBG-1(T16P) (J) and RBG-1(E22V) (K) restores the SQST-1::GFP accumulation in *epg-5; rbg-1* double mutants. (L) Quantification of the fluorescence intensity of SQST-1::GFP is shown as mean±s.e.m. (*n*=5). ****P*<0.001 (two-tailed *t*-test); ns, no significant difference. Scale bar: 20 µm (I–K). (M–P) In *bec-1(bp613)* hypomorphic mutants, a few SQST-1::GFP aggregates accumulate in embryos (N). (M) DIC image of the embryo in N. (O) Loss of *rbg-1* activity increases the number of SQST-1::GFP aggregates in *bec-1* mutants. (P) Quantification of the number of SQST-1::GFP aggregates in the indicated genetic backgrounds is shown as mean±s.e.m. (*n*=5). ***P*<0.01, ****P*<0.001 (two-tailed *t*-test). Scale bar: 10 µm (M–O). (Q–T) A few SQST-1::GFP aggregates accumulate in the head region of *cpl-1* mutants (R). (Q) DIC image of the animal in R. (S) *cpl-1; rbg-1* double mutants contain fewer SQST-1::GFP aggregates than *cpl-1* single mutant. (T) Quantification of the number of SQST-1::GFP in wild type, *cpl-1* mutants and *cpl-1; rbg-1* mutants is shown as mean±s.e.m. (*n*=7). ****P*<0.001 (two-tailed *t*-test). Scale bar: 20 µm (Q–S).

sfGFP::mCherry and/or acidification of lysosomes. We also examined lysosomal acidification using the NUC-1::pHTomato reporter, which is driven by the heat shock promoter. pHTomato is highly sensitive to pH and the fluorescence intensity is weaker in lower pH compartments (Li and Tsien, 2012). At 24 h after heat shock, the fluorescence signal of lysosomal-localized NUC-1::pHTomato was weaker in *rbg-1* mutants than in wild-type animals (Fig. 3I,J,O), indicating that lysosomal acidification is enhanced by loss of *rbg-1* activity.

Loss of function of *rbg-1* suppresses the impaired lysosomal function in *epg-5* mutants

In *epg-5* mutants, in addition to small spherical structures, NUC-1::mCherry labeled abnormally enlarged structures (Fig. 3C). GFP::RAB-7 also labeled enlarged structures, and there were fewer GFP-positive tubular structures (Fig. S3F). In *epg-5; rbg-1* double mutants, the number of abnormally enlarged GFP::RAB-7-labeled or NUC-1::mCherry-labeled structures was reduced, accompanied by formation of more small spherical and tubular structures, resembling the phenotype in *rbg-1* single mutants (Fig. 3D,M,N; Fig. S3G). EM analysis also showed that *epg-5* mutants contained enlarged lysosomal structures and small lysosomes with abnormal appearance in the hypodermis (Fig. 3G; Fig. S3M,N). Both of these phenotypes were suppressed by simultaneous depletion of *rbg-1* (Fig. 3H). We further determined whether loss of *rbg-1* activity restored the lysosomal function in *epg-5* mutants. Compared to wild-type animals, *epg-5* mutants exhibited a defect in NUC-1::sfGFP::mCherry delivery and/or acidification, and many yellow puncta persisted at 24 h after heat shock (Fig. 4K–O,E1). In *epg-5; rbg-1* double mutants, the delivery of NUC-1::sfGFP::mCherry was similar to *rbg-1* mutants and the GFP signal disappeared at 24 h after heat shock (Fig. 4P–T,E1). Compared to wild-type animals, the

Journal of Cell Science (2019) 132, jcs234195. doi:10.1242/jcs.234195

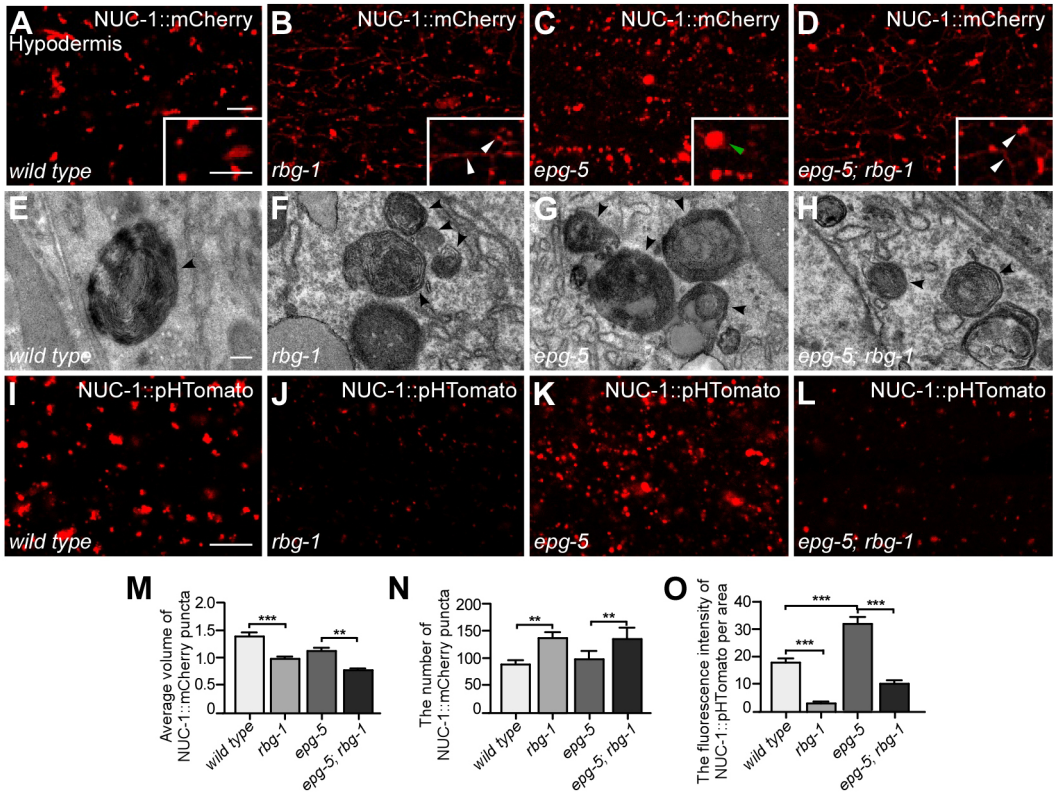

Fig. 3. Loss of function of *rbg-1* promotes lysosomal activity and suppresses the impaired lysosomal function in *epg-5* mutants. (A–D) NUC-1::mCherry forms spherical structures in wild-type animals (A). (B) More NUC-1::mCherry-labeled small spherical structures and tubular structures are present in *rbg-1* mutants. (C) NUC-1::mCherry labels abnormal enlarged structures in *epg-5* mutants. (D) In *epg-5; rbg-1* double mutants, NUC-1::mCherry labels more small spherical structures and tubular structures than in *epg-5* single mutants. White arrowheads indicate small spherical and tubular lysosome structures. The green arrowhead indicates an abnormal lysosome structure in *epg-5* mutants. Scale bar: 5 µm (A–D). (E–H) Compared to lysosomes in the hypodermis in wild-type animals (E), the lysosomes in *rbg-1* mutants are smaller and more abundant (F). (G) In addition to large hybrid vesicles, *epg-5* mutants also contain small lysosomes with abnormal morphology, possibly due to impaired degradation. (H) The lysosomes in *epg-5; rbg-1* double mutants resemble those in *rbg-1* mutants. Lysosomal structures are indicated by arrowheads. Scale bar: 200 nm (E–H). (I–L) The fluorescence intensity of NUC-1::pHTomato indicates the level of lysosomal acidification. Compared to wild-type animals (I), the fluorescence intensity of NUC-1::pHTomato is weaker in *rbg-1* mutants (J), and stronger in *epg-5* mutants (K). In *epg-5; rbg-1* double mutants, the fluorescence of NUC-1::pHTomato is similar to that in *rbg-1* single mutants (L). Scale bar: 5 µm (I–L). (M,N) Quantification of the volume (M) and the number (N) of NUC-1::mCherry-labeled spherical structures in wild-type, *rbg-1*, *epg-5*, *epg-5; rbg-1* animals. Data are shown as mean±s.e.m. (n=10). **P<0.01, ***P<0.001 (two-tailed t-test). (O) Quantification of the fluorescence intensity of NUC-1::pHTomato in the indicated genotypes. Data are shown as mean±s.e.m. (n=10). ***P<0.001 (two-tailed t-test).

fluorescence signal of NUC-1::pHTomato was stronger in *epg-5* mutants (Fig. 3K,O), indicating that lysosomal acidification is impaired in *epg-5* mutants. The enhanced fluorescence intensity of NUC-1::pHTomato in *epg-5* mutants was suppressed by loss of function of *rbg-1* (Fig. 3L,O). Taken together, these results provide evidence that loss of *rbg-1* activity suppresses the defect in lysosomal acidification in *epg-5* mutants.

In *epg-5* mutants, non-degradative autolysosomes are labeled by markers for a variety of endosomal vesicles (Wang et al., 2016). The recycling endosomal marker GFP::RAB-10 labeled a few punctate structures in the hypodermis of wild-type and *rbg-1* animals (Fig. S3H,I). GFP::RAB-10 labeled enlarged puncta in *epg-5* mutants, and this was suppressed in *epg-5; rbg-1* double mutants (Fig. S3J–L). In wild-type and *rbg-1* animals, BFP::LGG-1 formed a few small puncta that were separable from GFP::RAB-10-labeled structures (Fig. 5A,B,G). In *epg-5* mutants, BFP::LGG-1 labeled big puncta that largely co-localized with the enlarged NUC-1::mCherry- and GFP::RAB-10-labeled structures (Fig. 5C,G) (Wang et al., 2016). The number of enlarged LGG-1-labeled structures was dramatically reduced and their co-localization with GFP::RAB-10-labeled punctate structures also decreased in *epg-5; rbg-1* double mutants (Fig. 5D,G). These results indicated that formation of abnormally enlarged vesicles with mixed identities in *epg-5* mutants is suppressed by loss of *rbg-1* activity.

Loss of *rbg-1* activity suppresses the defect in dynamics of late endosome- and lysosome-associated RAB-7 in *epg-5* mutants

To determine the relative levels of GDP- and GTP-bound RAB-7, we examined the levels of RAB-7 in worm extracts that are pulled down by RILP, a RAB7 effector that specifically binds to GTP-bound RAB7 (Frasa et al., 2010). RAB-7 is conserved from *C. elegans* to mammals. GST–RILP interacted with RAB-7(Q68L), which mimics the active GTP-bound RAB-7, but not with RAB-7(T23N), which mimics the GDP-bound inhibitory form (Fig. S3O, P). The GST pulldown results showed that levels of GTP-bound RAB-7 were lower in *rbg-1* mutants than in wild-type worms (Fig. 6A,B), suggesting a concomitant increase in levels of the GDP-bound form of RAB-7 in *rbg-1* mutants. Levels of GTP-bound RAB-7 in *epg-5; rbg-1* mutants were similar to *rbg-1* single mutants (Fig. 6A,B). The purified RBG-1–RBG-2 complex did not show evidence of RAB-7 GEF activity (Fig. S3Q). Consistent with

Journal of Cell Science (2019) 132, jcs234195. doi:10.1242/jcs.234195

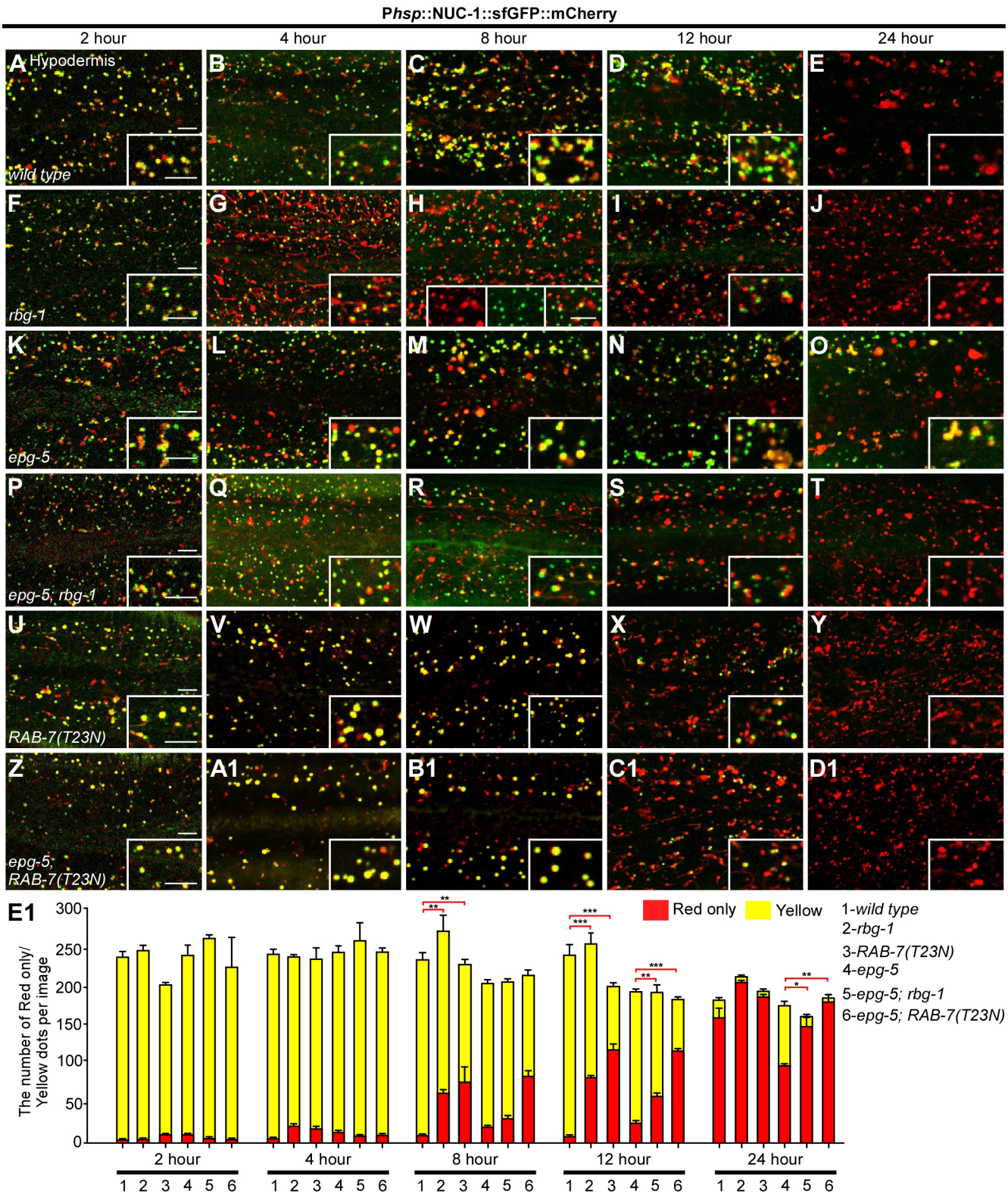

Fig. 4. See next page for legend.

this, no interaction was detected between GST–RAB-7(T23N) and TRX–RBG-1 (Fig. S3R). These results suggest that RBG-1 does not act as a GEF to regulate RAB-7 activity.

In wild-type worms, the ring-like structures of GFP::RAB-7 enclosed the punctate structures formed by NUC-1, indicating that GFP::RAB-7 is membrane-associated (Fig. S3S). We performed a fluorescence recovery after photobleaching (FRAP) assay to examine the mobility of membrane-associated GFP-RAB-7. In wild-type and *rbg-1* mutant hypodermis, the GFP–RAB-7 fluorescence signal recovered within 5 s after bleaching (Fig. 6C,D).

Journal of Cell Science (2019) 132, jcs234195. doi:10.1242/jcs.234195

Fig. 4. Loss of *rbg-1* activity and expression of RAB-7(T23N) accelerates the delivery of NUC-1::sfGFP::mCherry into lysosomes. (A–E) Expression pattern of NUC-1::sfGFP::mCherry at different time points after heat shock in wild-type animals. (A) At 2 h after heat shock, many puncta show both green and red signals. The green-only puncta are likely due to the faster folding of sfGFP than mCherry. (B–D) The number of red-only puncta increases after 12 h. (E) The GFP signal almost completely disappears after 24 h. (F–J) In *rbg-1* mutants, the green and red signals of NUC-1::sfGFP::mCherry are detected 2 h after heat shock (F). (I) The GFP dots largely disappear after 12 h. (H) Some mCherry puncta that co-localize with GFP dots are very faint. (K–O) In *epg-5* mutants, the green and red signals of NUC-1::sfGFP::mCherry are detected 2 h after heat shock (K). (O) A large number of yellow puncta persists even 24 h after heat shock. (P–T) The persistence of the GFP signal of NUC-1::sfGFP::mCherry in *epg-5* mutants at 24 h after heat shock is suppressed by loss of *rbg-1* activity. The pattern of NUC-1::sfGFP::mCherry in *epg-5; rbg-1* double mutants resembles that in *rbg-1* single mutants. (U–Y) The quenching of the GFP signal of NUC-1::sfGFP::mCherry is faster in animals expressing RAB-7(T23N). The green and red signals of NUC-1::sfGFP::mCherry are detected 2 h after heat shock (U), and the yellow puncta decrease with time (V,W). (X) The yellow puncta largely disappear 12 h after heat shock. (Z–D1) Expression of RAB-7(T23N) in *epg-5* mutants suppresses the persistent GFP signal of NUC-1::sfGFP::mCherry 24 h after heat shock. (E1) Quantification of the number of red-only and yellow puncta in wild-type, *rbg-1*, *RAB-7(T23N)*, *epg-5*, *epg-5; rbg-1* and *epg-5; RAB-7(T23N)* animals at different recovery times. Data are shown as mean±s.e.m. (n=5 per time point). *P<0.05, **P<0.01, ***P<0.001 (two-tailed t-test). (A–D1) are confocal images. Scale bar: 5 µm (A-D1).

However, the GFP–RAB-7 signal barely recovered in *epg-5* mutants (Fig. 6C,D). Simultaneous loss of function of *rbg-1* rescued the recovery of GFP–RAB-7 fluorescence in *epg-5* mutants after bleaching (Fig. 6C,D). These results indicate that loss of *rbg-1* activity promotes the mobility of RAB-7 on late endosomes and lysosomes in *epg-5* mutants.

Expression of GDP-bound RAB-7(T23N) suppresses the autophagy defect in *epg-5* mutants

We further investigated whether expression of the GDP-bound mutant RAB-7(T23N) suppresses the autophagy and lysosome defect in *epg-5* mutants. A low concentration of constructs expressing RAB-7(T23N) or RAB-7(Q68L) was injected and stable transgenic lines were obtained for analysis. No evident accumulation of SQST-1::GFP aggregates and GFP::LGG-1 puncta was detected in animals expressing RAB-7(T23N) or RAB-7(Q68L) (Fig. S4A–C). Expression of RAB-7(T23N), but not RAB-7(Q68L), suppressed the accumulation of SQST-1::GFP and GFP::LGG-1 puncta in *epg-5* mutants (Fig. 6E–N; Fig. S4D). The increased number of SQST-1::GFP aggregates in *cpl-1* mutants was also suppressed by RAB-7(T23N), but not by RAB-7(Q68L) (Fig. 6O–S). Expression of RAB-7(T23N) and RAB-7(Q68L) failed to suppress the autophagy defect in *scav-3* mutants (Fig. S4E).

We next examined whether expression of RAB-7(T23N) affects lysosomal biogenesis and function in *epg-5* mutants. NUC-1::mCherry labeled more small spherical structures in animals expressing RAB-7(T23N) (Fig. 6U; Fig. S4G). Expression of RAB-7(Q68L) had no evident effect on the pattern of NUC-1::mCherry-labeled structures (Fig. S4H). The delivery rate of NUC-1::sfGFP::mCherry was faster in animals expressing RAB-7(T23N), and resembled *rbg-1* mutants (Fig. 4U–Y,E1). LGG-1 formed a few puncta that were separate from GFP::RAB-10-labeled structures in animals expressing RAB-7(T23N) (Fig. 5E,G). Expression of RAB-7(T23N), but not RAB-7(Q68L), suppressed the accumulation of abnormal NUC-1::mCherry-labeled structures in *epg-5* mutants (Fig. 6T–X). The defective delivery rate of NUC-1::sfGFP::mCherry and the co-localization of BFP::LGG-1 with NUC-1::mCherry and GFP::RAB-10 in *epg-5* mutants were also suppressed by RAB-7(T23N) expression (Fig. 4Z–E1; Fig. 5F,G). These results indicated that expression of RAB-7(T23N), similar to loss of function of *rbg-1*, suppresses impaired autolysosome degradation in *epg-5* animals.

Different from RAB-7(T23N) expression, partial reduction of *rab-7* activity using RNAi enhanced the accumulation of SQST-1::GFP aggregates in *epg-5* single mutants and *epg-5; rbg-1* double mutants (Fig. S4J,K). *rab-7(RNAi)* animals contained numerous small NUC-1::mCherry-labeled structures, suggesting a defect in lysosomal formation (Fig. S4I). These results indicate that suppression of the defect in *epg-5* mutants by expression of RAB-7(T23N) does not occur through reduction of RAB-7 activity.

DISCUSSION

Loss of *rbg-1* activity promotes lysosomal function and suppresses the accumulation of non-functional autolysosomes associated with *epg-5* depletion

Here, we have uncovered a novel role of the RBG-1–RBG-2 complex in modulating lysosomal biogenesis and function. Compared to wild-type animals, *rbg-1* mutants contain more spherical and tubular late endosomes and lysosome structures. Loss of *rbg-1* activity accelerates lysosomal maturation and degradation, as shown by the enhanced delivery of the lysosomal enzyme NUC-1, attenuation of the impaired degradation in *cpl-1* mutants, and suppression of the autophagy defect and accumulation of enlarged non-degradative autolysosomes in *epg-5* mutants. The RAB3GAP1–RAB3GAP2 complex has been shown to act as a GAP for RAB3 to regulate neurotransmitter release and synaptic plasticity (Sakane et al., 2006; Müller et al., 2011). The RAB3GAP1–RAB3GAP2 complex also localizes to subdomains of the endoplasmic reticulum (ER) and functions as a GEF for RAB18 (Gerondopoulos et al., 2014). This complex is also localized on lipid droplets (LDs) and is required for targeting and activation of RAB18 on LDs for LD growth and maturation (Xu et al., 2018). The RAB3GAP1–RAB3GAP2 complex has been shown to modulate autophagosomal biogenesis and its loss of function enhances protein aggregation in muscle cells in a manner dependent on the GAP activity but not on RAB3 itself (Spang et al., 2014). The *Drosophila* ortholog of RBG-1 (CG31935) is also required for autophagy in muscle (Zirin et al., 2015). Consistent with this, we found that loss of *rbg-1* activity slightly increases accumulation of SQST-1 aggregates in *bec-1* hypomorphic mutants. The suppression effect of RBG-1 on the autophagy defect in *epg-5* mutants is independent of its GAP and GEF activity. Thus, the RBG-1–RBG-2 complex has dual functions in autophagy.

The dynamics of membrane-associated RAB-7 controls lysosomal biogenesis and function

RAB7 regulates multiple processes involving late endosomes and also plays a key role in lysosomal biogenesis (Bucci et al., 2000; Wang et al., 2011; Hyttinen et al., 2013; Guerra and Bucci, 2016; Wong et al., 2018). Biogenesis and maintenance of the lysosomal compartment requires the concerted actions of lysosome fission, and also of heterotypic fusion of late endocytic vesicles with pre-existing lysosomes. RAB7 controls homotypic fusion of late endosomes and their heterotypic fusion with lysosomes. The proper function of RAB7 requires a precise balance of the activated and inactivated forms (Frasa et al., 2010; Carroll et al., 2013). Overexpression of the GTP-bound form of RAB7 increases the fusion and thus the size of lysosomes, and also causes their perinuclear localization, while expression of the inhibitory mutant form of RAB7 results in dispersal

Journal of Cell Science (2019) 132, jcs234195. doi:10.1242/jcs.234195

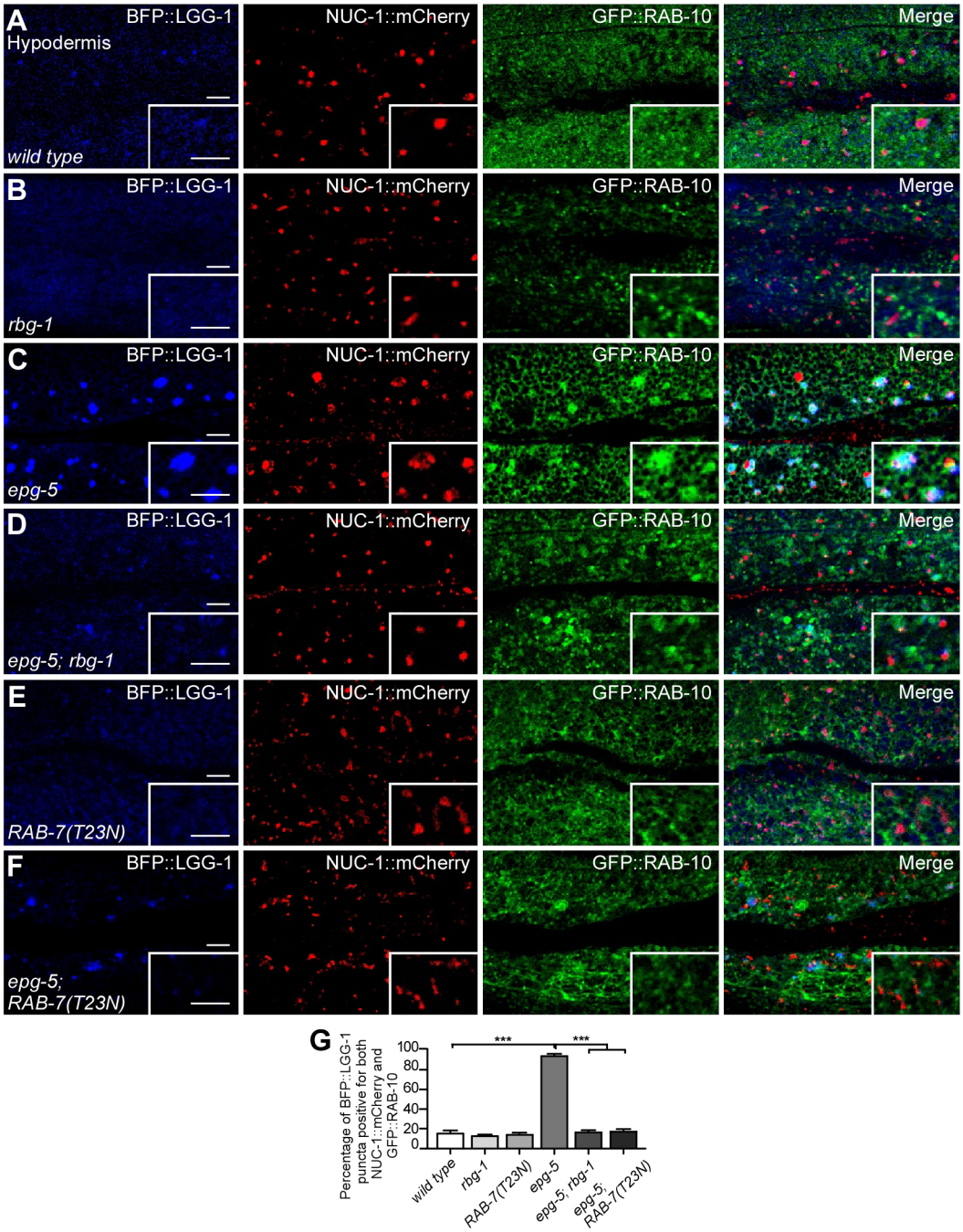

Fig. 5. Loss of function of *rbg-1* suppresses the non-specific fusion of autophagosomes with various endocytic vesicles in *epg-5* mutants. (A,B) BFP::LGG-1 forms a few small dots that are separate from GFP::RAB-10-labeled structures in wild-type (A) and *rbg-1* (B) animals. (C) In *epg-5* mutants, BFP::LGG-1 forms enlarged punctate structures that are largely co-localized with NUC-1::mCherry- and GFP::RAB-10-labeled structures. (D) In *epg-5; rbg-1* double mutants, the formation of enlarged BFP::LGG-1 puncta is decreased and the colocalization of BFP::LGG-1 with both NUC-1::mCherry and GFP::RAB-10 is also reduced. (E) In animals expressing RAB-7(T23N), a few BFP::LGG-1 puncta are separate from GFP::RAB-10-labeled structures. (F) Expression of RAB-7(T23N) suppresses the accumulation of enlarged BFP::LGG-1 puncta in *epg-5* mutants. The co-localization of BFP::LGG-1 with NUC-1::mCherry and GFP::RAB-10 is also reduced by RAB-7(T23N) expression. Scale bars: 5 µm (A–F). (G) Quantification of the percentage of BFP::LGG-1 puncta positive for both NUC-1::mCherry and GFP::RAB-10 in the indicated genotypes. Data are shown as mean±s.e.m. (n=5). ***P<0.001 (two-tailed t-test).

of lysosomes (Bucci et al., 2000). Elevated RAB7-GTP levels in *Vps34*-deficient cells, which results from failed recruitment of the PI(3)P-binding RAB7 GAP Armus (also known as TBC1D2) to late endosomes, causes the formation of enlarged late endosomes and impaired lysosomal maturation (Jaber et al., 2016).

The GEF for regulating RAB-7 on lysosomes has yet to be identified. The MON1–CCZ1 complex, which is a RAB5 effector, is involved in the recruitment and activation of RAB7 on late endosomes (Kinchen and Ravichandran, 2010; Nordmann et al., 2010; Poteryaev et al., 2010). The MON1–CCZ1 complex dissociates from late endosomes prior to their fusion with lysosomes, and thus is not involved in RAB7 activation on lysosomes (Poteryaev et al., 2010; Yasuda et al., 2016). The RBG-1–RBG-2 complex appears to have been newly revealed to act as a

Journal of Cell Science (2019) 132, jcs234195. doi:10.1242/jcs.234195

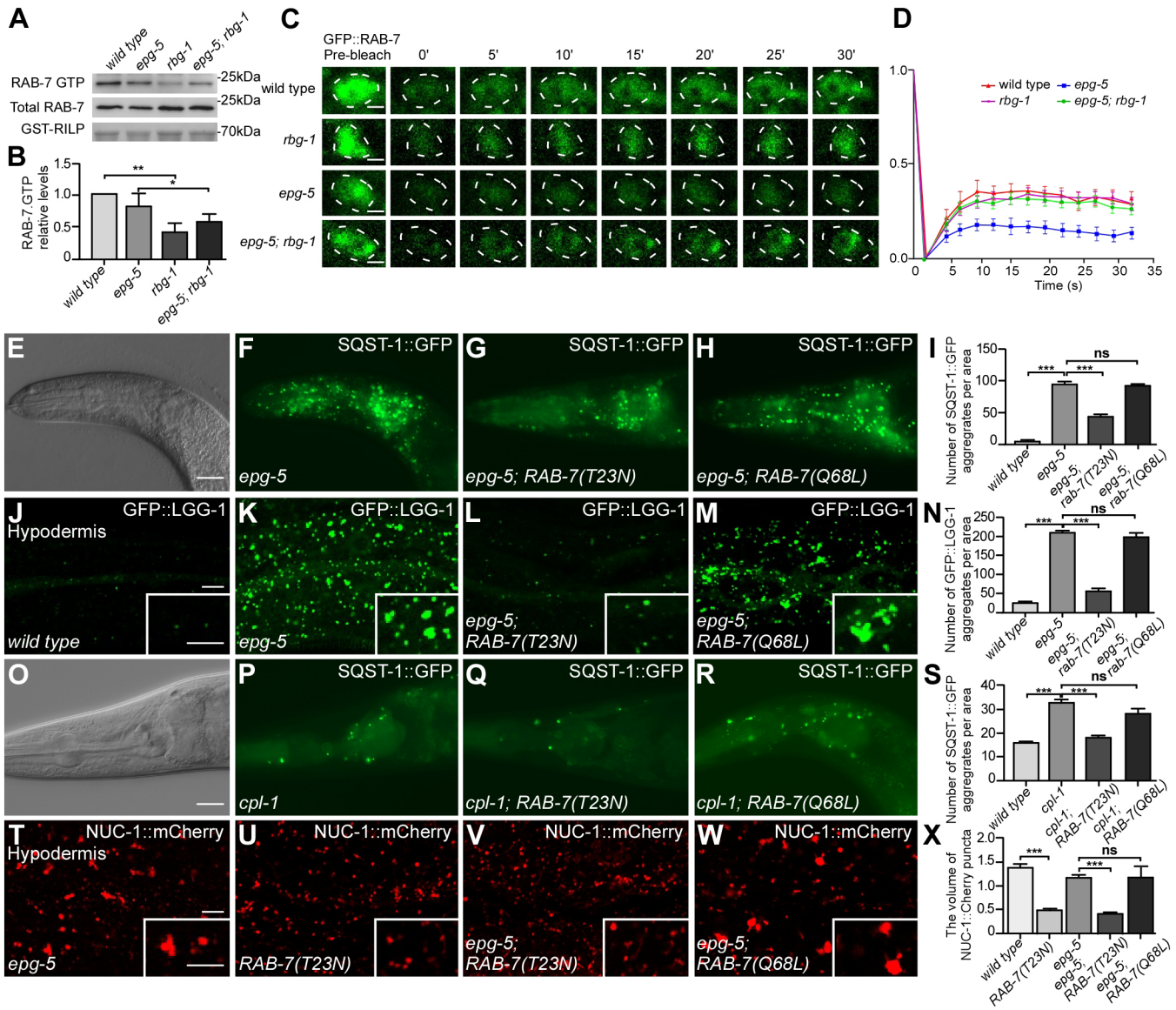

Fig. 6. Expression of GDP-bound RAB-7(T23N) suppresses the autophagy defect in *epg-5* mutants. (A) In a GST pulldown assay, levels of GTP-bound endogenous RAB-7 pulled down by GST–RILP are lower in *rbg-1* and *epg-5; rbg-1* worm extracts than wild-type and *epg-5* worm extracts. (B) Quantification of the level of RAB-7 GTP in wild type, *epg-5*, *rbg-1* and *epg-5; rbg-1*. Data are shown as mean±s.e.m. (n=3). *P<0.05, **P<0.01 (two-tailed t-test). Levels of GTP-bound RAB-7 are normalized to total RAB-7 in the corresponding animals and compared to the level in wild-type animals, which is set to 1.0. (C) In wild-type and *rbg-1* animals, the fluorescence signal of GFP–RAB-7 recovers after photobleaching. Recovery of the GFP–RAB-7 after photobleaching is poor in *epg-5* mutants, while it is much more efficient in *epg-5; rbg-1* double mutants. The photobleached area is outlined. Scale bar: 1 µm. (D) Recovery of GFP–RAB-7 fluorescence after photobleaching in wild type, *rbg-1*, *epg-5* and *epg-5; rbg-1* mutants (n=6). Data are shown as mean±s.e.m. (E–I) A large number of SQST-1::GFP aggregates accumulate in the head region of *epg-5* mutants (F). (E) DIC image of the animal in F. Expression of RAB-7(T23N) (G), but not RAB-7(Q68L) (H) suppresses the accumulation of SQST-1::GFP in *epg-5* mutants. (I) Quantification of the number of SQST-1::GFP aggregates in wild type, *epg-5*, *epg-5; RAB-7(T23N)* and *epg-5; RAB-7(Q68L)* is shown as mean±s.e.m. (n=5). ***P<0.001 (two-tailed t-test); ns, no significant difference. Scale bar: 20 µm (E–H). (J–N) GFP::LGG-1 is largely diffuse and only forms a few small puncta in wild-type hypodermis (J), while it accumulates into numerous puncta in *epg-5* mutants (K). Expression of RAB-7(T23N) (L), but not RAB-7(Q68L) (M), suppresses the accumulation of GFP::LGG-1 puncta in *epg-5* animals. (N) Quantification of the number of GFP::LGG-1 puncta in the indicated genotypes is shown as mean±s.e.m. (n=5). ***P<0.001 (two-tailed t-test); ns, no significant difference. Scale bar: 5 µm (J–M). (O–S) SQST-1::GFP aggregates accumulate in the head region of *cpl-1* mutants (P). (O) DIC image of the animal in P. Expression of RAB-7(T23N) (Q), but not RAB-7(Q68L) (R) suppresses the accumulation of SQST-1::GFP aggregates in *cpl-1* mutants. (S) Quantification of the number of SQST-1::GFP aggregates in the indicated genotypes. Data are shown as mean±s.e.m. (n=6). ***P<0.001 (two-tailed t-test); ns, no significant difference. Scale bar: 20 µm (O–R). (T–X) In *epg-5* mutants, NUC-1::mCherry labels abnormally enlarged structures (T). NUC-1::mCherry forms many small spherical structures in RAB-7(T23N)-expressing animals (U). Expression of RAB-7(T23N) (V), but not RAB-7(Q68L) (W), suppresses the abnormal NUC-1::mCherry-labeled structures in *epg-5* mutants. (X) Quantification of the volume of NUC-1::mCherry spherical structures in wild-type, *RAB-7(T23N)*, *epg-5*, *epg-5; RAB-7(T23N)* and *epg-5; RAB-7(Q68L)* animals is shown as mean±s.e.m. (n=8). ***P<0.001 (two-tailed t-test); ns, no significant difference. Scale bars: 5 µm (T–W).

RAB-7 regulator to modulate lysosome biogenesis and function. Levels of GTP-bound RAB-7 are lower in *rbg-1* mutants than wild-type animals. Expression of RAB-7(T23N) mimics loss of *rbg-1* activity in facilitating lysosomal biogenesis. One possible function of wild-type RBG-1 could be to target the RAB-7 GEF to lysosomes, or to promote its activity on lysosomes.

Journal of Cell Science (2019) 132, jcs234195. doi:10.1242/jcs.234195

In the autophagy pathway, autophagosomes and/or amphisomes fuse with lysosomes to form degradative autolysosomes. Upon degradation of the sequestrated materials, lysosomes are regenerated from autolysosomes (Yu et al., 2010). The activity of RAB7 is precisely controlled to ensure the progression of autophagic flux. Depletion of the RAB7 GAP Armus impairs autolysosome formation and acidification (Carroll et al., 2013). RAB7 knockout cells show accumulation of autolysosomes, indicating that RAB7 is essential for autolysosome maturation (Kuchitsu and Fukuda, 2018). In EPG5-depleted cells or *epg-5* mutant animals, GFP::RAB7 forms abnormally enlarged punctate structures (Wang et al., 2016). The reduced mobility of GFP::RAB-7 on late endosomes and lysosomes in *epg-5* mutants may recruit effectors such as HOPS to promote fusion. Accumulation of active GTP-bound RAB-7 on autolysosomes also depletes the availability of cycling and/or mobile RAB-7 and causes a defect in non-lysosomal functions of RAB-7, such as delivery of lysosomal enzymes. Loss of *rbg-1* activity or expression of the GDP inhibitory form of RAB-7 promotes the dynamics of membrane-associated RAB-7 in *epg-5* mutants. The release of RAB-7 from autolysosomes promotes the transport of lysosomal enzymes and/or lysosomal membrane proteins to increase the acidification of lysosomes. These effects restore the autolysosome function and ameliorate the autophagy defect in *epg-5* mutants. Accumulation of non-degradative autolysosomes has been observed in Vici syndrome patient tissues (Cullup et al., 2013). Our study provides new insights into potential therapeutic treatments of Vici syndrome.

MATERIALS AND METHODS

Worm strains

Strains of *C. elegans* were cultured and maintained on nematode growth medium (NGM) according to standard protocols (Brenner, 1974) at 20°C unless indicated otherwise. The Hawaiian strain CB4856 was used for polymorphism mapping.

The following strains were used in this work: N2 Bristol (wild-type), *epg-5(tm3425)*, *rbg-1(bp1150)*, *bec-1(bp613)*, *epg-7(tm2508)*, *rpl-43(bp399)*, *cpl-1(qx304)*, *scav-3(qx193)*, *bpIs267(*P_{hyp-7}SQST-1::GFP*, unc-76)*, *bpIs262(*P_{ges-1}SQST-1::GFP*, unc-76)*, *bpIs151(*P_{sqst-1}SQST-1::GFP*, unc-76)*, *bpIs193(*P_{hlh-1}SQST-1::GFP*, unc-76)*, *bpIs328(*$P_{unc-119}$SQST-1::GFP*, unc-76)*, *adIs2122(*P_{lgg-1}GFP::LGG-1*, rol-6(su1006))*, *bpEx342(*P_{hyp-7}BFP::LGG-1, P_{myo-2}::GFP*)*, *qxIs686(*P_{hyp-7}GFP::RAB-10*, unc-76)*, *qxIs66(*P_{ced-1}GFP::RAB-7*, unc-76)*, *qxIs257(*P_{ced-1}NUC-1::mCherry*, unc-76)*, *qxIs750(*P_{hsp}NUC-1::pHTomato, P_{ord-1}::GFP), *qxIs612(*P_{hsp}NUC-1::sfGFP::mCherry*, unc-76)* and *bpIs395(*P_{nfya-1}RAB-7(T23N)*, rol-6(su1006))*. Further details are provided in Table S1.

bec-1(bp613) contains an aspartic acid to asparagine mutation at amino acid 347. The autophagy defect in *bec-1(bp613)* is much weaker than in *bec-1(ok700)* null mutants.

Mapping and cloning of *rbg-1*

Mapping using genetic and SNP markers placed *bp1150* on chromosome X, between 21.23 cM and 21.97 cM. A transgene containing fosmid WRM0637bE01 or the single gene *rbg-1* restored the accumulation of SQST-1 aggregates in *epg-5; bp1150* mutants.

Transgene expression

Constructs were injected into worms at a concentration of ∼20 ng/µl to obtain stable transgenic lines. Transgenes analyzed in this study include: P_{hyp-7}::RBG-1, P_{hyp-7}::RBG-1(R667A), P_{hyp-7}::RBG-1(T16P), P_{hyp-7}::RBG-1(E22V), P_{nfya-1}::RAB-7(T23N) and P_{nfya-1}::RAB-7(Q68L). Further details are provided in Table S1.

RNAi inactivation experiments

For RNAi injection experiments, single-stranded RNA was transcribed from T7 and SP6 promoter-flanked PCR templates. ssRNAs were annealed and injected into wild-type animals or animals carrying the indicated transgene. The F1 progeny at the indicated developmental stages were examined for the phenotype.

The primers used for RNAi synthesis were: *lgg-1* 5′-CACTAGTAATACGACTCACTATAGGGATGAAGTGGGCTTACAAGG-3′, 5′-CACTAGATTTAGGTGACACTATAGAACCTTCTTTTCGACCTCTCCT-3′; *rbg-1* 5′-CACTAGTAATACGACTCACTATAGGGCTTGAACCGAACAACGAAGG-3′, 5′-CACTAGATTTAGGTGACACTATAGAAGCATCAAGTGGACCTTCATG-3′; *rbg-2* 5′-CACTAGTAATACGACTCACTATAGGGGGAAATGTTCGGGTATGTGC-3′, 5′-CACTAGATTTAGGTGACACTATAGAACATCAATATCCTCTTGAGAC-3′; *rab-18* 5′-CACTAGTAATACGACTCACTATAGGGGCGTGGATTTCCGCGTAACT-3′, 5′-CACTAGATTTAGGTGACACTATAGAACTAGCATCCACACATTCC-3′; *rab-7* 5′-CACTAGTAATACGACTCACTATAGGGATGTCGGGAACCAGAAAGA-3′, 5′-CACTAGATTTAGGTGACACTATAGAACTGGAGATTCTCTAGCCAACG-3′.

Generation of CRISPR/Cas9 knockout mutants in *C. elegans*

Mutations in *rab-3* were generated by CRISPR/Cas9. sgRNA was injected into *epg-5; rbg-1* animals with a co-injection marker and F1 progeny were examined. The sgRNA sequence was 5′-CCAATCTTCGAAGGGTTC-3′. In *rab-3(bp1558)* mutants, five nucleotides (TCGTC) were deleted, which introduced a premature stop codon at amino acid 101 (RAB-3 contains 220 amino acid residues).

Protein expression and purification

All genes were PCR-amplified and cloned into the pET.32M.3C vector to produce TRX–His6-tag-fused recombinant proteins, or the pGEX.6p-1 vector to produce GST-tag-fused recombinant proteins. Point mutations were introduced by the site-directed mutagenesis approach (Landt et al., 1990).

Soluble recombinant proteins were expressed in *Escherichia coli* BL21-CodenPlus (DE3) and purified on glutathione Sepharose 4B beads (for GST-tagged proteins, GE Healthcare) and Ni-NTA agarose beads (for His6-tagged proteins, Qiagen). After extensive washing, the proteins were eluted with a buffer containing 1×PBS (140 mM NaCl, 2.7 mM KCl, 10 mM Na_2HPO_4, 1.8 mM KH_2PO_4) and 10 mM L-glutathione (Sigma-Adrich, 70-18-8) (for GST-tagged proteins), and 50 mM HEPES (pH 7.9), 500 mM imidazole and 500 mM NaCl (for His6-tagged proteins). The eluted proteins were then loaded onto a desalting column (GE Healthcare, 17-0851-01) and finally eluted with 1×PBS buffer.

We failed to purify *E. coli* expressed RBG-2. Adult worms expressing FLAG–RBG-1 and FLAG–RBG-2 were collected and lysed in lysis buffer containing 25 mM HEPES pH 7.4, 150 mM NaCl, 0.5% NP40, 1 mM EDTA, 10% glycerol, 1 mM DTT and protease inhibitor cocktail (EDTA-free; Roche, B14003). The worm extracts were clarified by centrifugation at 18,000 ***g*** for 30 min at 4°C. The FLAG-tagged proteins were isolated from the clarified worm lysate using 100 µl anti-FLAG M2 affinity gel (Sigma-Aldrich, A2220) for 4 h at 4°C. The beads were washed five times with worm washing buffer (25 mM HEPES pH 7.4, 300 mM NaCl, 1 mM EDTA, 0.5% NP40, 10% glycerol), and ten times with GEF reaction buffer (20 mM HEPES pH 6.8, 1 mg/ml BSA, 150 mM NaCl, 1 mM $MgCl_2$). The proteins were separated on 10% SDS-PAGE gels for analysis by immunoblotting. The proteins bound to FLAG beads were snap-frozen in liquid nitrogen for storage at −80°C and prepared for the nucleotide exchange assay.

In vitro pulldown assays

Glutathione Sepharose 4B beads (GST, GE Healthcare, 17-0756-05) were washed in pulldown buffer (140 mM NaCl, 2.7 mM KCl, 10 mM Na_2HPO_4, 1.8 mM KH_2PO_4 and 1% NP-40) three times. 20–30 µg GST and GST-tagged proteins were incubated with 20 µl GST beads in 500 µl pulldown buffer for 0.5 h at 4°C. The supernatants were then removed. The GST beads were washed three times with pulldown buffer. 50 µg Trx-tagged proteins were incubated with the GST-tagged protein-conjugated beads in 500 µl pulldown buffer for 1 h at 4°C. The beads were then washed three times with pulldown buffer and the bound proteins were boiled in 5×SDS sample loading buffer and visualized by means of immunoblotting. To determine the interaction of RILP or RBG-1 with constitutively active GTP-

bound mutant RAB proteins *in vitro*, GTP and Mg^{2+} were added to the buffer. For the interaction with dominant-negative GDP-bound mutant RAB proteins, GDP was added to the buffer. To examine the level of GTP-bound RAB-7 in wild type and mutants, GST–RILP bound to GST beads was incubated with worm extracts. Antibody against RAB-7 (1:1000; Chen et al., 2010) and secondary antibody (peroxidase AffiniPure goat anti-rat IgG, Jackson ImmunoResearch, 112-035-003) were used to detect the level of endogenous GTP-bound RAB-7 in worm extracts.

Fluorescence recovery after photobleaching assay

Animals expressing GFP–RAB-7 were cultured at 20°C and young adult animals (24 h after L4 stage) were used for analysis. The FRAP assay was performed using a confocal microscope (LSM 880 Meta plus Zeiss Axiovert zoom, Zeiss) using a 63× oil immersion objective lens (Plan-Apochromatlan, Zeiss) at room temperature. The selected regions of interest were bleached at 488 nm and the fluorescence intensities in these regions were collected every 2.5 s. The pre-bleach intensity was used to normalize the fluorescence intensity. Image intensity was measured by mean regions of interest (ROI), calculated using ZEN software and analyzed by Prism (GraphPad).

Immunoblotting assay

The samples were subjected to SDS-PAGE and signals were detected with diluted polyclonal rat anti-RAB-7 (Chen et al., 2010) and monoclonal mouse anti-Trx-tag (Genscript, A00180-40) primary antibodies (diluted 1:1000, unless specifically indicated) and peroxidase AffiniPure goat anti-rat IgG (Jackson ImmunoResearch, 112-035-003), HRP-goat anti-mouse (Jackson ImmunoResearch, 115-035-003) secondary antibodies (diluted 1:200).

Indirect immunofluorescence assay

Embryos were collected by cutting 50–100 gravid animals. The embryos were permeabilized using the freeze-cracking method, and fixed with methanol and acetone (−20°C), then blocked with PBS (140 mM NaCl, 2.7 mM KCl, 10 mM Na_2HPO_4, 2 mM KH_2PO_4, 1% BSA) for 1 h and incubated with polyclonal rat anti-PGL-3 (1:1000; Zhang et al., 2009), polyclonal rabbit anti-SEPA-1 (1:10,000; Zhang et al., 2009), polyclonal rat anti-SQST-1 (also known as T12G3.1; 1:1000; Tian et al., 2010) and polyclonal rat anti-LGG-1 (1:1000; Tian et al., 2010) primary antibodies overnight at 4°C. The embryos were then washed three times with PBST (PBS+0.2% tween 20) and incubated for 1 h with FITC-conjugated AffiniPure goat anti-rat IgG (Jackson ImmunoResearch, 112-095-003) or rhodamine-conjugated goat anti-rabbit IgG (Jackson ImmunoResearch, 111-025-003) and Alexa Fluor 594 AffiniPure goat anti-rat IgG (Jackson ImmunoResearch, 112-585-003) secondary antibodies (diluted 1:200) at 20°C. The embryos were then washed three times with PBST and stained with DAPI before examination.

Nucleotide exchange assays

2′-(3′)-bis-O-(N-methylanthraniloyl)-GDP (Mant-GDP) (Jena Bioscience, Germany) was loaded with 10 nmol of hexahistidine-GST-RAB in a buffer (20 mM HEPES pH 6.8, 1 mg/ml BSA, 20 mM EDTA pH 8.0, 40 mM Mant-GDP) at 30°C for 30 min. Next, 25 mmol $MgCl_2$ was added and Zeba spin columns (Fisher Scientific) were used to exchange the sample into reaction buffer (20 mM HEPES pH 6.8, 1 mg/ml BSA, 150 mM NaCl, 1 mM $MgCl_2$). This step removes the free Mant-GDP. Nucleotide exchange was measured using 1 nmol of the loaded RAB and the amount of GEF specified in the figure legends in a final volume of 100 µl reaction buffer by monitoring the quenching of fluorescence after release of Mant-GDP using a Tristar LB 941 plate reader (Berthold Technologies, UK) under control of MikroWin software (Qiagen, 9234701). Samples were excited at 350 nm and emission was monitored at 440 nm. GTP was added to a final concentration of 0.1 mM to start the exchange reaction at 30°C. Data were collected using a Safire multimode microplate spectrophotometer (Tecan) and plotted and analyzed using Microsoft Excel (Delprato et al., 2004).

Quantification of lysosome volume

Young adult animals (24 h post-L4 larval stage) expressing NUC-1::mCherry were mounted on agar pads in buffer with 5 mM levamisole. Fluorescent images in 15–20 *z*-series (0.5 µm/section) were taken with a spinning-disk confocal scanner unit (UltraView, PerkinElmer) using a 100× oil immersion objective (CFI Plan Apochromat Lambda, NA 1.45, Nikon) at room temperature. Serial optical sections were analyzed. The volume of NUC-1::mCherry-positive lysosomes was analyzed with Velocity software (PerkinElmer). At least 10 animals for each genotype were quantified and the data was analyzed using Prism (GraphPad).

Imaging, quantification and statistical analysis

Images were taken using Zeiss Axio Imager M2 and LSM880 microscopes. Imaging was carried out on animals at the same developmental stage, and on a similar body region of each animal. The same exposure time and magnification were used for comparison. Immunoblots were representative of three independent experiments. Images were analyzed using Image J. Statistical analysis was carried out using GraphPad Prism5 software and significant differences between datasets were determined by performing Student's *t*-test (two-tailed). The results are shown as mean±s.e.m. $*P<0.05$, $**P<0.01$, $***P<0.001$.

Acknowledgements

We are grateful to Dr Isabel Hanson for editing work and members of Hong Zhang's lab for helpful discussion.

Competing interests

The authors declare no competing or financial interests.

Author contributions

Conceptualization: H. Zhang, X.W.; Methodology: Z.W., C.Y., H. Zhao; Validation: Z.W., H. Zhao; Formal analysis: H. Zhang, Z.W.; Investigation: Z.W.; Resources: Z.W., C.Y., D.Z., Y.S., X.W.; Data curation: Z.W., H. Zhao; Writing - original draft: H. Zhang, Z.W.; Writing - review & editing: H. Zhang; Visualization: H. Zhang, Z.W., H. Zhao; Supervision: H. Zhang; Project administration: H. Zhang; Funding acquisition: H. Zhang.

Funding

This work was supported by the National Natural Science Foundation of China (NSFC) (31421002, 31561143001, 31630048 and 31790403), by Beijing Municipal Science and Technology Commission (Z181100001318003), by the National Chinese Ministry of Science and Technology (2017YFA0503401), by the Strategic Priority Research Program of the Chinese Academy of Sciences (CAS) (grant XDB19000000) and Key Research Program of Frontier Sciences, CAS (grant QYZDY-SSW-SMC006) to H. Zhang. The research is also partly supported by University of Chinese Academy of Sciences Education Foundation Fountain-Valley Life Sciences Fund.

Supplementary information

Supplementary information available online at
http://jcs.biologists.org/lookup/doi/10.1242/jcs.234195.supplemental

References

Bas, L., Papinski, D., Licheva, M., Torggler, R., Rohringer, S., Schuschnig, M. and Kraft, C. (2018). Reconstitution reveals Ykt6 as the autophagosomal SNARE in autophagosome-vacuole fusion. *J. Cell Biol.* **217**, 3656-3669. doi:10.1083/jcb.201804028

Blümer, J., Rey, J., Dehmelt, L., Mazel, T., Wu, Y.-W., Bastiaens, P., Goody, R. S. and Itzen, A. (2013). RabGEFs are a major determinant for specific Rab membrane targeting. *J. Cell Biol.* **200**, 287-300. doi:10.1083/jcb.201209113

Brenner, S. (1974). The genetics of Caenorhabditis elegans. *Genetics* **77**, 71-94.

Bucci, C., Thomsen, P., Nicoziani, P., McCarthy, J. and van Deurs, B. (2000). Rab7: a key to lysosome biogenesis. *Mol. Biol. Cell* **11**, 467-480. doi:10.1091/mbc.11.2.467

Carroll, B., Mohd-Naim, N., Maximiano, F., Frasa, M. A., McCormack, J., Finelli, M., Thoresen, S. B., Perdios, L., Daigaku, R., Francis, R. E. et al. (2013). The TBC/RabGAP Armus coordinates Rac1 and Rab7 functions during autophagy. *Dev. Cell* **25**, 15-28. doi:10.1016/j.devcel.2013.03.005

Chen, B., Jiang, Y., Zeng, S., Yan, J., Li, X., Zhang, Y., Zou, W. and Wang, X. (2010). Endocytic sorting and recycling require membrane phosphatidylserine asymmetry maintained by TAT-1/CHAT-1. *PLoS Genet.* **6**, e1001235. doi:10.1371/journal.pgen.1001235

Cullup, T., Kho, A. L., Dionisi-Vici, C., Brandmeier, B., Smith, F., Urry, Z., Simpson, M. A., Yau, S., Bertini, E., McClelland, V. et al. (2013). Recessive mutations in EPG5 cause Vici syndrome, a multisystem disorder with defective autophagy. *Nat. Genet.* **45**, 83-87. doi:10.1038/ng.2497

Delprato, A., Merithew, E. and Lambright, D. G. (2004). Structure, exchange determinants, and family-wide rab specificity of the tandem helical bundle and Vps9 domains of Rabex-5. *Cell* **118**, 607-617. doi:10.1016/j.cell.2004.08.009
Dionisi, V. C., Sabetta, G., Gambarara, M., Vigevano, F., Bertini, E., Boldrini, R., Parisi, S. G., Quinti, I., Aiuti, F. and Fiorilli, M. (1998). Agenesis of the corpus callosum, combined immunodeficiency, bilateral cataract, and hypopigmentation in two brothers. *Am. J. Med. Genet.* **29**, 1-8. doi:10.1002/ajmg.1320290102
Feng, Y., He, D., Yao, Z. and Klionsky, D. J. (2014). The machinery of macroautophagy. *Cell Res.* **24**, 24-41. doi:10.1038/cr.2013.168
Frasa, M. A. M., Maximiano, F. C., Smolarczyk, K., Francis, R. E., Betson, M. E., Lozano, E., Goldenring, J., Seabra, M. C., Rak, A., Ahmadian, M. R. et al. (2010). Armus is a Rac1 effector that inactivates Rab7 and regulates E-cadherin degradation. *Curr. Biol.* **20**, 198-208. doi:10.1016/j.cub.2009.12.053
Fukui, K., Sasaki, T., Imazumi, K., Matsuura, Y., Nakanishi, H. and Takai, Y. (1997). Isolation and characterization of a GTPase activating protein specific for the Rab3 subfamily of small G proteins. *J. Biol. Chem.* **272**, 4655-4658. doi:10.1074/jbc.272.8.4655
Gao, J., Langemeyer, L., Kümmel, D., Reggiori, F. and Ungermann, C. (2018a). Molecular mechanism to target the endosomal Mon1-Ccz1 GEF complex to the pre-autophagosomal structure. *eLife* **7**, e31145. doi:10.7554/eLife.31145
Gao, J., Reggiori, F. and Ungermann, C. (2018b). A novel in vitro assay reveals SNARE topology and the role of Ykt6 in autophagosome fusion with vacuoles. *J. Cell Biol.* **217**, 3670-3682. doi:10.1083/jcb.201804039
Gerondopoulos, A., Bastos, R. N., Yoshimura, S., Anderson, R., Carpanini, S., Aligianis, I., Handley, M. T. and Barr, F. A. (2014). Rab18 and a Rab18 GEF complex are required for normal ER structure. *J. Cell Biol.* **205**, 707-720. doi:10.1083/jcb.201403026
Guerra, F. and Bucci, C. (2016). Multiple roles of the small GTPase Rab7. *Cells* **5**, E34. doi:10.3390/cells5030034
Guo, B., Huang, X., Zhang, P., Qi, L., Liang, Q., Zhang, X., Huang, J., Fang, B., Hou, W., Han, J. et al. (2014). Genome-wide screen identifies signaling pathways that regulate autophagy during Caenorhabditis elegans development. *EMBO Rep.* **15**, 705-713. doi:10.1002/embr.201338310
Hegedűs, K., Takáts, S., Boda, A., Jipa, A., Nagy, P., Varga, K., Kovács, A. L. and Juhász, G. (2016). The Ccz1-Mon1-Rab7 module and Rab5 control distinct steps of autophagy. *Mol. Biol. Cell* **27**, 3132-3142. doi:10.1091/mbc.e16-03-0205
Hyttinen, J. M. T., Niittykoski, M., Salminen, A. and Kaarniranta, K. (2013). Maturation of autophagosomes and endosomes: a key role for Rab7. *Biochim. Biophys. Acta* **1833**, 503-510. doi:10.1016/j.bbamcr.2012.11.018
Itakura, E., Kishi-Itakura, C. and Mizushima, N. (2012). The hairpin-type tail-anchored SNARE syntaxin 17 targets to autophagosomes for fusion with endosomes/lysosomes. *Cell* **151**, 1256-1269. doi:10.1016/j.cell.2012.11.001
Jaber, N., Mohd-Naim, N., Wang, Z., DeLeon, J. L., Kim, S., Zhong, H., Sheshadri, N., Dou, Z., Edinger, A. L., Du, G. et al. (2016). Vps34 regulates Rab7 and late endocytic trafficking through recruitment of the GTPase-activatingprotein Armus. *J. Cell Sci.* **129**, 4424-4435. doi:10.1242/jcs.192260
Jiang, P., Nishimura, T., Sakamaki, Y., Itakura, E., Hatta, T., Natsume, T. and Mizushima, N. (2014). The HOPS complex mediates autophagosome-lysosome fusion through interaction with syntaxin 17. *Mol. Biol. Cell* **25**, 1327-1337. doi:10.1091/mbc.e13-08-0447
Kinchen, J. M. and Ravichandran, K. S. (2010). Identification of two evolutionarily conserved genes regulating processing of engulfed apoptotic cells. *Nature* **464**, 778-782. doi:10.1038/nature08853
Kuchitsu, Y. and Fukuda, M. (2018). Revisiting Rab7 functions in mammalian autophagy: Rab7 knockout studies. *Cells* **7**, E215. doi:10.3390/cells7110215
Landt, O., Grunert, H. P., and Hahn, U. (1990). A general method for rapid site-directed mutagenesis using the polymerase chain reaction. *Gene* **96**, 125-128. doi:10.1016/0378-1119(90)90351-q
Langemeyer, L., Fröhlich, F. and Ungermann, C. (2018). Rab GTPase function in endosome and lysosome biogenesis. *Trends Cell Biol.* **28**, 957-970. doi:10.1016/j.tcb.2018.06.007
Li, Y. and Tsien, R. W. (2012). pHTomato, a red, genetically encoded indicator that enables multiplex interrogation of synaptic activity. *Nat. Neurosci.* **15**, 1047-1053. doi:10.1038/nn.3126
Li, Y., Chen, B., Zou, W., Wang, X., Wu, Y., Zhao, D., Sun, Y., Liu, Y., Chen, L., Miao, L. et al. (2016). The lysosomal membrane protein SCAV-3 maintains lysosome integrity and adult longevity. *J. Cell Biol.* **215**, 167-185. doi:10.1083/jcb.201602090
Lin, L., Yang, P., Huang, X., Zhang, H., Lu, Q. and Zhang, H. (2013). The scaffold protein EPG-7 links cargo-receptor complexes with the autophagic assembly machinery. *J. Cell Biol.* **201**, 113-129. doi:10.1083/jcb.201209098
Lu, Q., Yokoyama, C. C., Williams, J. W., Baldridge, M. T., Jin, X., DesRochers, B., Bricker, T., Wilen, C. B., Bagaitkar, J., Loginicheva, E. et al. (2016). Homeostatic control of innate lung inflammation by vici syndrome gene Epg5 and additional autophagy genes promotes influenza pathogenesis. *Cell Host Microbe.* **19**, 102-113. doi:10.1016/j.chom.2015.12.011
Matsui, T., Jiang, P., Nakano, S., Sakamaki, Y., Yamamoto, H. and Mizushima, N. (2018). Autophagosomal YKT6 is required for fusion with lysosomes independently of syntaxin 17. *J. Cell Biol.* **217**, 2633-2645. doi:10.1083/jcb.201712058
McEwan, D. G., Popovic, D., Gubas, A., Terawaki, S., Suzuki, H., Stadel, D., Coxon, F. P., Miranda de Stegmann, D., Bhogaraju, S., Maddi, K. et al. (2015). PLEKHM1 regulates autophagosome- lysosome fusion through HOPS complex and LC3/GABARAP proteins. *Mol. Cell* **57**, 39-54. doi:10.1016/j.molcel.2014.11.006
Mizuno-Yamasaki, E., Rivera-Molina, F. and Novick, P. (2012). GTPase networks in membrane traffic. *Annu. Rev. Biochem.* **81**, 637-659. doi:10.1146/annurev-biochem-052810-093700
Müller, M., Pym, E. C. G., Tong, A. and Davis, G. W. (2011). Rab3-GAP controls the progression of synaptic homeostasis at a late stage of vesicle release. *Neuron* **69**, 749-762. doi:10.1016/j.neuron.2011.01.025
Nagano, F., Sasaki, T., Fukui, K., Asakura, T., Imazumi, K. and Takai, Y. (1998). Molecular cloning and characterization of the noncatalytic subunit of the Rab3 subfamily-specific GTPase-activating protein. *J. Biol. Chem.* **273**, 24781-24785. doi:10.1074/jbc.273.38.24781
Nakatogawa, H., Suzuki, K., Kamada, Y. and Ohsumi, Y. (2009). Dynamics and diversity in autophagy mechanisms: lessons from yeast. *Nat. Rev. Mol. Cell Biol.* **10**, 458-467. doi:10.1038/nrm2708
Nordmann, M., Cabrera, M., Perz, A., Bröcker, C., Ostrowicz, C., Engelbrecht-Vandré, S. and Ungermann, C. (2010). The Mon1-Ccz1 complex is the GEF of the late endosomal Rab7 homolog Ypt7. *Curr. Biol.* **20**, 1654-1659. doi:10.1016/j.cub.2010.08.002
Poteryaev, D., Datta, S., Ackema, K., Zerial, M. and Spang, A. (2010). Identification of the switch in early-to-late endosome transition. *Cell* **141**, 497-508. doi:10.1016/j.cell.2010.03.011
Sakane, A., Manabe, S., Ishizaki, H., Tanaka-Okamoto, M., Kiyokage, E., Toida, K., Yoshida, T., Miyoshi, J., Kamiya, H., Takai, Y. et al. (2006). Rab3 GTPase-activating protein regulates synaptic transmission and plasticity through the inactivation of Rab3. *Proc. Natl. Acad. Sci. USA* **103**, 10029-10034. doi:10.1073/pnas.0600304103
Spang, N., Feldmann, A., Huesmann, H., Bekbulat, F., Schmitt, V., Hiebel, C., Koziollek-Drechsler, I., Clement, A. M., Moosmann, B., Jung, J. et al. (2014). RAB3GAP1 and RAB3GAP2 modulate basal and rapamycin-induced autophagy. *Autophagy* **10**, 2297-2309. doi:10.4161/15548627.2014.994359
Stenmark, H. (2009). Rab GTPases as coordinators of vesicle traffic. *Nat. Rev. Mol. Cell Biol.* **10**, 513-525. doi:10.1038/nrm2728
Tian, Y., Li, Z., Hu, W., Ren, H., Tian, E., Zhao, Y., Lu, Q., Huang, X., Yang, P., Li, X. et al. (2010). C. elegans screen identifies autophagy genes specific to multicellular organisms. *Cell* **141**, 1042-1055. doi:10.1016/j.cell.2010.04.034
Vaites, L. P., Paulo, J. A., Huttlin, E. L. and Harper, J. W. (2017). Systematic analysis of human cells lacking ATG8 proteins uncovers roles for GABARAPs and the CCZ1/MON1 regulator C18orf8/RMC1 in macroautophagic and selective autophagic flux. *Mol. Cell. Biol.* **38**, e00392-17. doi:10.1128/MCB.00392-17
Wandinger-Ness, A. and Zerial, M. (2014). Rab proteins and the compartmentalization of the endosomal system. *Cold Spring Harb. Perspect. Biol.* **6**, a022616. doi:10.1101/cshperspect.a022616
Wang, T., Ming, Z., Xiaochun, W. and Hong, W. (2011). Rab7: role of its protein interaction cascades in endo-lysosomal traffic. *Cell. Signal.* **23**, 516-521. doi:10.1016/j.cellsig.2010.09.012
Wang, Z., Miao, G. Y., Xue, X., Guo, X. Y., Yuan, C. Z., Wang, Z. Y., Zhang, G. M., Chen, Y. Y., Feng, D., Hu, J. J. et al. (2016). The vici syndrome protein EPG5 Is a Rab7 effector that determines the fusion specificity of autophagosomes with late endosomes/lysosomes. *Mol. Cell* **63**, 781-795. doi:10.1016/j.molcel.2016.08.021
Wong, Y. C., Ysselstein, D. and Krainc, D. (2018). Mitochondria-lysosome contacts regulate mitochondrial fission via RAB7 GTP hydrolysis. *Nature* **554**, 382-386. doi:10.1038/nature25486
Xu, D., Li, Y., Wu, L., Li, Y., Zhao, D., Yu, J., Huang, T., Ferguson, C., Parton, R. G., Yang, H. et al. (2018). Rab18 promotes lipid droplet (LD) growth by tethering the ER to LDs through SNARE and NRZ interactions. *J. Cell Biol.* **217**, 975-995. doi:10.1083/jcb.201704184
Yasuda, S., Morishita, S., Fujita, A., Nanao, T., Wada, N., Waguri, S., Schiavo, G., Fukuda, M. and Nakamura, T. (2016). Mon1-Ccz1 activates Rab7 only on late endosomes and dissociates from the lysosome in mammalian cells. *J. Cell Sci.* **129**, 329-340. doi:10.1242/jcs.178095
Yu, L., McPhee, C. K., Zheng, L., Mardones, G. A., Rong, Y., Peng, J., Mi, N., Zhao, Y., Liu, Z., Wan, F. et al. (2009). Termination of autophagy and reformation of lysosomes regulated by mTOR. *Nature* **465**, 942-946. doi:10.1038/nature09076
Zhang, Y., Yan, L., Zhou, Z., Yang, P., Tian, E., Zhang, K., Zhao, Y., Li, Z., Song, B., Han, J. et al. (2009). SEPA-1 mediates the specific recognition and degradation of P granule components by autophagy in C. *elegans*. *Cell* **136**, 308-321. doi:10.1016/j.cell.2008.12.022
Zhao, Y. G. and Zhang, H. (2019). Autophagosome maturation: an epic journey from the ER to lysosomes. *J. Cell Biol.* **218**, 757-770. doi:10.1083/jcb.201810099
Zhao, H., Zhao, Y. G., Wang, X., Xu, L., Miao, L., Feng, D., Chen, Q., Kovács, A. L., Fan, D. and Zhang, H. (2013a). Mice deficient in Epg5 exhibit selective neuronal vulnerability to degeneration. *J. Cell Biol.* **200**, 731-741. doi:10.1083/jcb.201211014
Zhao, Y. G., Zhao, H., Sun, H. and Zhang, H. (2013b). Role of Epg5 in selective neurodegeneration and Vici syndrome. *Autophagy* **9**, 1258-1262. doi:10.4161/auto.24856
Zirin, J., Nieuwenhuis, J., Samsonova, A., Tao, R. and Perrimon, N. (2015). Regulators of autophagosome formation in Drosophila muscles. *PLoS Genet.* **11**, e1005006. doi:10.1371/journal.pgen.1005006